Experimental Mechanics
DOI 10.1007/s11340-017-0315-x

BRIEF TECHNICAL NOTE

Quasi-Static and Dynamic Large Strain Shear-Tension Testing

A. Dorogoy[1] · **D. Rittel**[1]

Received: 19 March 2017 / Accepted: 3 July 2017

Abstract A new shear specimen is designed, evaluated and tested quasi-statically and dynamically. The specimen consists of a long cylinder having a horizontal gauge section created by two diametrically opposed semi-circular slots machined parallel to the longitudinal axis. This geometry imposes a rather uniform stress state, close to pure shear in the gauge section. Quasi-static and dynamic tension-shear tests up to a strain rate of 10^4 1/s were carried out on 1020 cold-drawn steel specimens. The obtained stress–strain curves and ductility were validated numerically. The new specimen can be used to study the shear mechanical characteristics of a material using tensile testing.

Keywords Large strain · Shear-tension · Quasi static testing · Dynamic testing · Steel 1020

Introduction

The true stress–strain curves and ductility of materials are needed for accurate numerical simulations in diverse areas such as ballistic impact, crashworthiness, machining, forming, frictional effects, erosion and seismic faulting [1, 2]. These properties are dependent on strain-rate, temperature, triaxiality and Lode parameter, not always available in the literature. To generate these properties, extensive research work has been conducted [3–11].

✉ A. Dorogoy
Dorogoy@technion.ac.il

[1] Faculty of Mechanical Engineering, Technion – Israel Institute of Technology, 32000 Haifa, Israel

A wide spectrum of test specimens have been developed to examine and quantify the shear propensity of materials [1, 11–13], but only a few are used with conventional quasi-static and dynamic testing machines alike. Among those, one should mention the hat-specimen [14–17], the shear-compression disc [18, 19], and others for sheet metals [20, 21].

In this study a new shear specimen is designed, evaluated and tested quasi-statically and dynamically. The shear specimen consists of a long cylinder having a horizontal gauge section created by two diametrically opposed semi-circular slots that are machined parallel to the longitudinal axis. This geometry allows for tests to be carried out both with a conventional uniaxial and Tensile Hopkinson Split Bar method (SHTB) [22]. The specimen and its data reduction is similar to the previously proposed shear compression specimen (SCS) [23, 24], and shear tension specimen (STS) [25].

Materials and Methods

Quasi-Static Tensional Tests

Six specimens (Fig.1(a)) were tested in tension in a servo-hydraulic machine (MTS) with a crosshead velocity of 0.5 mm/min. The extensional displacement (δu) and applied load (F) were measured. The extensional displacement was measured by a laser extensometer and is the distance between two reflectors located on both side of the specimen gauge at an initial gap of ~33 mm. The applied load was measured by the MTS load cell. The mounted specimen during test is shown in Fig. 1(b).

The experimental results are summarized in Fig. 2(a). The applied load in Fig. 2(a) is divided by the mid-section area of the gauge. There is a very good repeatability of the results

Published online: 20 July 2017

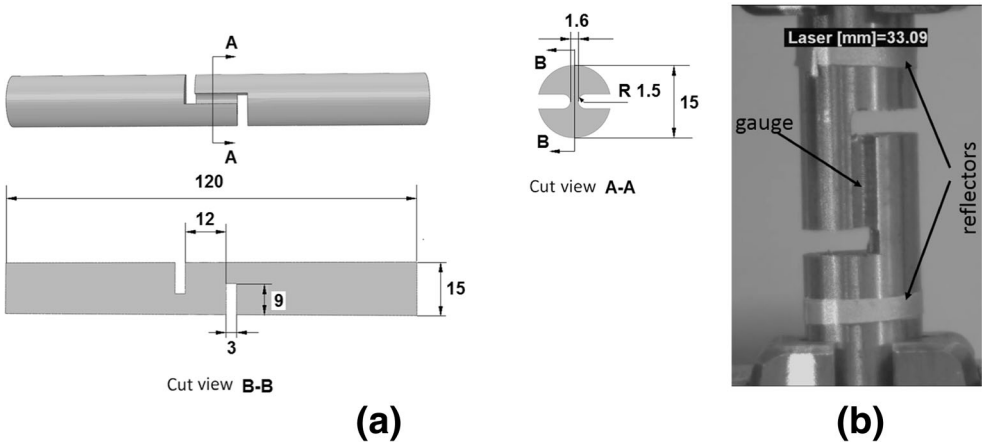

Fig. 1 (**a**) The quasi static specimen dimensions. (**b**) A mounted specimen in the MTS servo hydraulic machine

although specimen number 1 failed earlier, while specimen number 4 underwent slightly higher stresses.

The data reduction technique involves two phases of numerical simulations:

1) Pre-test simulation.
2) Verification.

Abaqus standard [26] is used for the pre-test simulations which are quasi-static, 3D, and use elastic-plastic material model with Mises plasticity. The applied material properties are taken from literature or previous test results with other specimens. The applied displacement (ΔU) is converted into averaged equivalent plastic strain on the mid-cut section, using $\widehat{\varepsilon_p} = f_1(\Delta U)$. The applied load (F) is converted to the averaged Mises stress on the mid-cut section using $\widehat{\sigma} = g(\widehat{\varepsilon})F$. The detailed formulas and coefficients are given in appendix 1.

The resulting stress-strain curve is shown in Fig. 2(b) by the dotted (blue) curve. This curve was extended linearly because there are points on the mid cut section that experience higher strains than the average strain which is predicted by the data reduction formulas. This curve serves as a first guess for the validation process.

The same numerical simulations are conducted during the validation phase. Slight changes to the material input of the predicted σ_{eq} - ε_p curve of Fig. 2(b) are added until a good agreement between the experimental and the numerical load-displacement curve is obtained. A ductile failure strain criterion [27] is added. This strain, ε_p^f, is changed systematically until a good agreement for the location of the failure on the load-displacement (Fig. 2(a)) is obtained. The validated σ - ε_p is shown in Fig. 2(b) by the red line. When this σ - ε_p relationship is used as input in the numerical simulations, a very good agreement between the numerical F/(Lt)-ΔU to the experimental ones is achieved. The numerical F/(Lt) - ΔU for three different failure strain: ε_p^f = 1.4, 1.5 and 1.6 are shown in Fig. 2(a). It can be observed that ε_p^f = 1.5 is an appropriate value for the ductility.

The triaxiality (t_r) and the Lode parameter (μ) are defined by equations (1–2) [28–30] as:

$$t_r = -\frac{p}{\sigma_e} \tag{1}$$

$$\mu = \frac{2\sigma_2 - \sigma_1 - \sigma_3}{\sigma_1 - \sigma_3} \tag{2}$$

Where the pressure (p) and the equivalent Mises stress (σ_e) are given in equations (3–4)

$$p = -\sigma_m = -\frac{1}{3}\sigma_{ii} = -\frac{1}{3}(\sigma_1 + \sigma_2 + \sigma_3) \tag{3}$$

$$\sigma_e = \sqrt{\frac{3}{2}s_{ij}s_{ij}} = \sqrt{\frac{1}{2}\left[(\sigma_1 - \sigma_2)^2 + (\sigma_2 - \sigma_3)^2 + (\sigma_3 - \sigma_1)^2\right]} \tag{4}$$

$$s_{ij} = \sigma_{ij} - \sigma_m I \tag{5}$$

The stresses $\sigma_1 > \sigma_2 > \sigma_3$ are the principal stresses.

Figure 2(c) shows the variation of the *averaged* triaxiality and Lode (t_r,μ) parameters during the plastic deformations. The triaxiality ranges from $0.015 < \widehat{t_r} < 0.165$ with an average of 0.083. The Lode parameter ranges from $-0.3145 < \widehat{\mu} < -0.0425$ with an average of −0.155. The low triaxiality and Lode parameter indicate that the the stress situation during plastic deformation is close to pure shear.

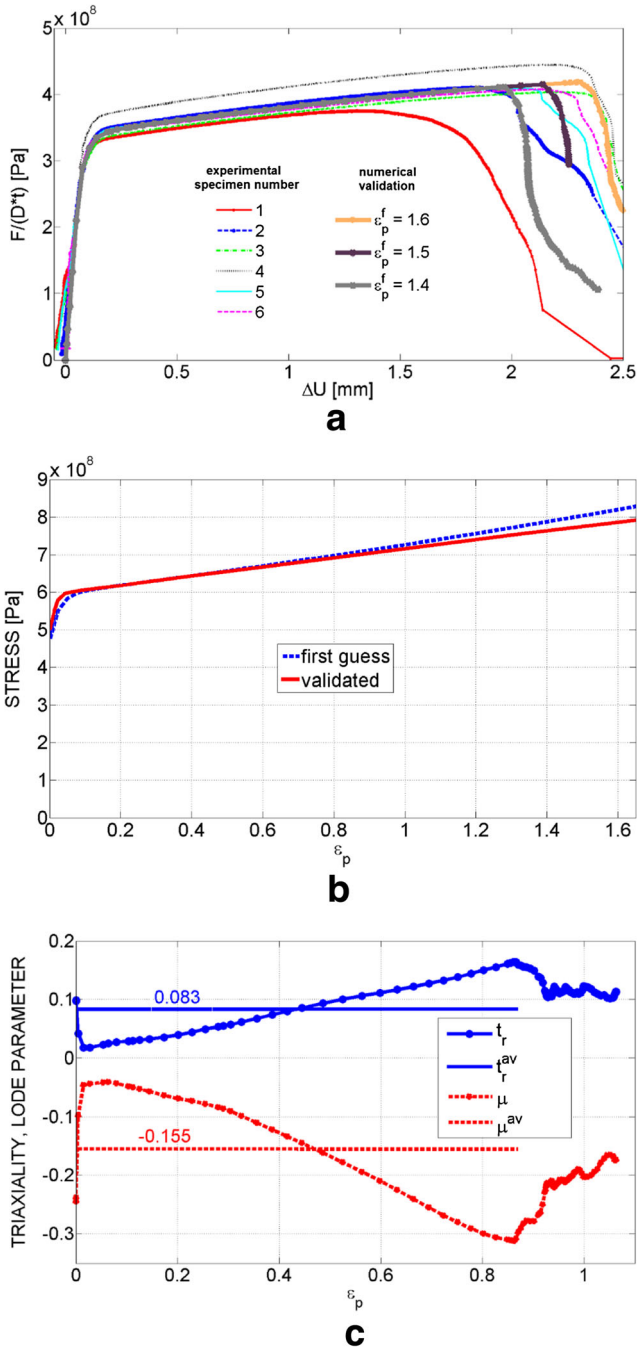

Fig. 2 (**a**) The six experimental F/(Lt) - ΔU in comparison to the numerical F/(Lt) - ΔU which is obtained by using the validated σ_{eq} - ε_p for 3 different failure strain: $\varepsilon_p^f = 1.4$, 1.5 and 1.6. (**b**) The validated σ - ε_p in comparison to the predicted σ - ε_p. (**c**) The variation of the averaged values on the mid cut section of the triaxiality and Lode paramater during loading. Note the average values during loading

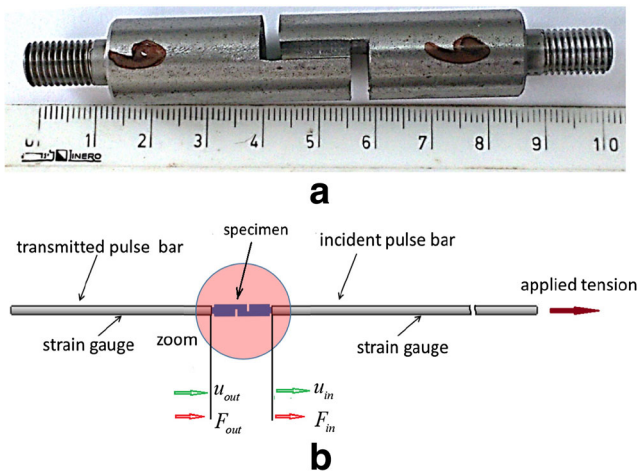

Fig. 3 (**a**) The shear specimen for dynamic testing. (**b**) A schematic draw of the SHTB showing the location of the specimen and the location of the obtained forces and displacements

Dynamic Tension Tests

Five shear specimens (Fig. 3(a)) were tested in a split Hopkinson tension bars apparatus (SHTB) [22], made of hardened C300 maraging steel tension bars. A sketch of the SHTB is shown in Fig. 3(b). The geometry of the specimens is similar to the quasi-static specimens (Fig. 1) with $D = 15\ mm$ but shorter length. The specimen is screwed on both sides to the bars using 5/16 UNF threads with 10 mm length.

The experimentally obtained F_{in} and F_{out} versus the applied displacement Δ (Δ = u_{in} - u_{out}) are shown in Fig. 4(a). A high degree of repeatability of the experimental results is noticeable. It can be observed that during the early stage of the pulse, up to approximately Δu = 0.97 mm, corresponding to ~80 μs, there is no dynamic load equilibrium; hence properties obtained in this time (or Δ) regime are not accurate.

The dynamic flow behavior and ductility of the shear specimen is obtained by hybrid numerical-experimental technique similar to the STS. We conducted a 3D nonlinear dynamic simulation of the experimental setup using Abaqus explicit [26]. An elastic material model was used for the SHTB bars (Appendix 2). An elastic-plastic Johnson–Cook (JC) material model was used for the 1020 steel (Appendix 2) specimen together with a ductile failure criterion [27].

We use here the JC material model [30] for identifying the dynamic σ-ε_p of the material. The flow stress σ_{eq} is assumed to be of the form:

$$\sigma_{eq} = \left[A + B(\varepsilon_p)^n\right]\left[1 + C\log\left(\frac{\dot{\varepsilon}_p}{\dot{\varepsilon}_p^r}\right)\right]\left[1-\Theta^m\right] \qquad (6)$$

with the usual definition of this model's parameters (Appendix 2).

We used the quasi-static curves shown in Fig. 2(b) to determine the parameters A,B and n: A = 500 MPa, B = 227 MPa and $n = 0.41$. The parameter m was set to 1.0

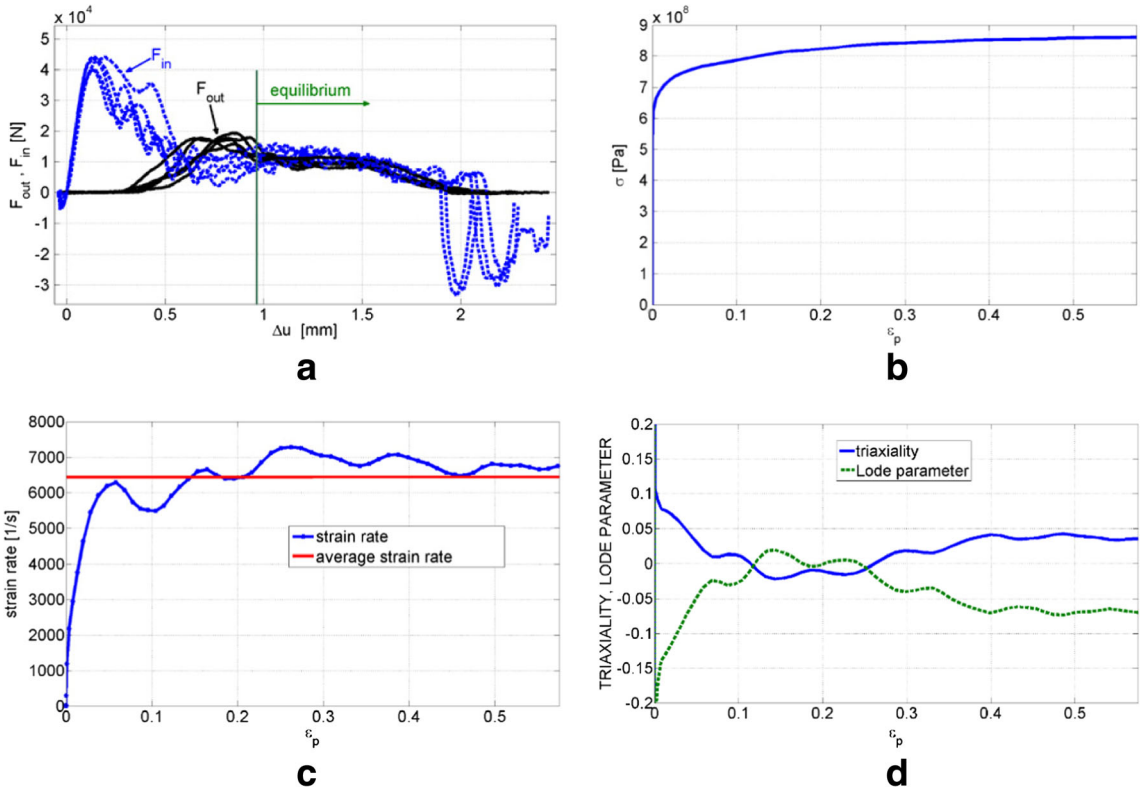

Fig. 4 (**a**) The experimentally obtained F_{in} and F_{out} versus Δ. (**b**) The averaged σ-ε_p in mid-section of the shear specimen gauge during dynamic shear. (**c**) The averaged strain rate vs. ε_p in mid-section of the shear specimen gauge during dynamic shear showing an average value of ~6500 1/s during impact. (**d**) The averaged triaxiality and Lode parameter vs. ε_p in mid-section of the shear specimen gauge during the dynamic shear

– common value for steel [31]. We assumed $\dot{\varepsilon}_p^r = 1$ and systematically changed C until a good agreement is obtained between the numerical and experimental F_{in} and F_{out}.

Figure 5(a) shows the converged (C = 0.04, ε_p^f = 0.8) numerical $F_{out}(\Delta)$ in comparison to five experimental curve. A good agreement is achieved for $\Delta > 1$ mm for which dynamic equilibrium exists (see Fig. 4(a)). The "overshoot" of the experimental $F_{out}(\Delta)$ for $\Delta < 1$ mm is probably due to inertial and thread-related effects [25], keeping in mind that the threads were not modelled explicitly. Numerical tests in which the material was assumed to have higher strength and a drop of strength were carried out. These tests denied this possibility since the resulting $F_{out}(\Delta)$ and $F_{in}(\Delta)$ were completely different from the measured ones. A few values of failure strain were tested numerically and the value of ε_p^f = 0.8 cause a best fit between the numerical and experimental F_{out} . The dynamic shear ductility is therefore 0.8. A good agreement between the converged numerical $F_{in}(\Delta)$ to the five experimentally measured ones is shown in Fig. 5(b).

A summary of the JC parameters of cold rolled 1020 steel as well as the elastic properties of the bars is given in Appendix 2.

The averaged σ-ε_p on the mid-section of the gauge during the impact is shown in Fig. 4(b). This curve is affected by the evolving strain rate and temperature during the impact. The corresponding strain rate is shown at Fig. 4(c). The strain rate reaches a maximum value of 7400 1/s at ε_p^f = 0.25 and has an average value of 6500 1/s. The averaged triaxiality and Lode parameter vs. ε_p on the mid-section of the gauge are shown in Fig. 4(d). It can be observed that their absolute value is lower than 0.05 for $\varepsilon_p > 0.05$, indicating a dynamic stress situation which is very close to pure shear.

Summary and Conclusions

A new shear specimen, inspired from [1, 21, 24, 25], is *designed, evaluated and tested in tension quasi-statically and dynamically*. The specimen geometry imposes a stress state in the gauge section that is close to pure shear. For 1020 cold drawn steel, the quasi-static ductility at (absolute value) of triaxiality and Lode parameter of ~0.1 is 1.5. The dynamic ductility at strain rate of ~6500 1/s was found to be 0.8, hence the high shear strain rate elevates the flow stress but lowers the dynamic ductility.

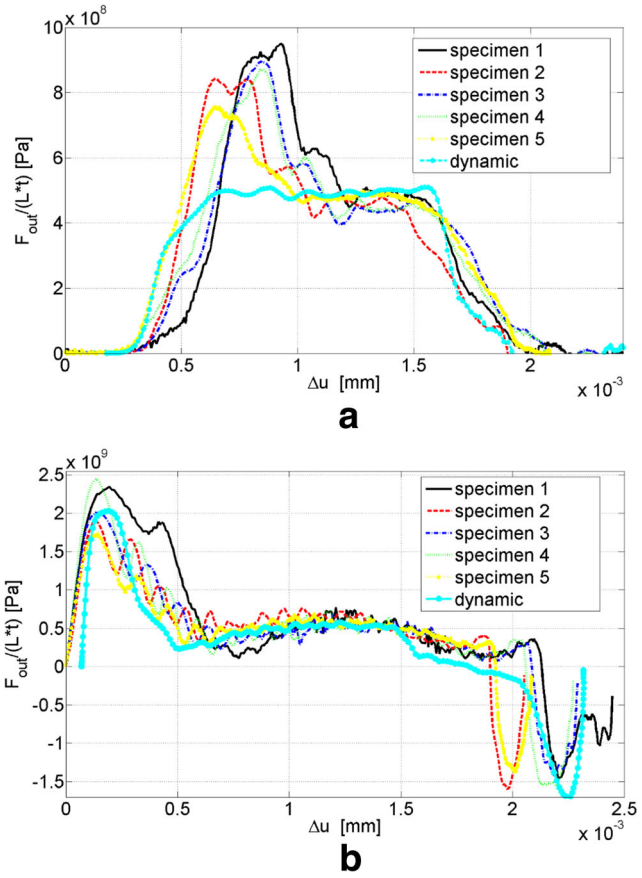

Fig. 5 (**a**) A comparison between experimental $F_{out}(\Delta)$ and the numerically converged $F_{out}(\Delta)$. (**b**) A comparison between experimental $F_{in}(\Delta)$ and the numerically converged $F_{in}(\Delta)$

The new specimen can be used to study the shear mechanical characteristics of a material at both low and high strain rates.

Acknowledgements Mr. A. Reuven and Mr. Y. Rozitski's assistance with the production of the specimens and conducting the experiments is greatly appreciated.

Appendix 1

The data reduction formulas

$$\widehat{\varepsilon_p} = k_1 \frac{\Delta U - \Delta U_y}{L} + k_2 \left(\frac{\Delta U - \Delta U_y}{L} \right)^2 \tag{7}$$

$$\widehat{\sigma} = \left[a e^{b\widehat{\varepsilon_p}} + c e^{d\widehat{\varepsilon_p}} \right] \frac{F}{L \cdot t} \tag{8}$$

In equations (7)–(8) the gauge length is L and the gauge thickness is t. The displacement at which the gauge start to yield is ΔU_Y. The coefficients k_1, k_2, a, b, c and d are detailed in Table 1.

Table 1 Coefficients for data reduction

k_1	k_2	a	b	c	d
6.872	−12.0	1.744	−0.04869	−0.05305	−7.706

Appendix 2

Summary of material properties used in numerical analyses.

Table 2 Material properties

	Steel 1020	C300 Managing steel
density ρ $\frac{Kg}{m^3}$	7870	8000
Young's modulus E GPa	205	184
Poisson's ratio ν	0.29	0.3
c m/s	5104	4800
Specific heat c_p $\frac{J}{Kg\,C^\circ}$	486	–
Inelastic heat fraction β	0.9	–

The Johnson-Cook material model is given by:

$$\sigma_{eq} = \left[A + B\left(\varepsilon_p\right)^n \right] \left[1 + C\log\left(\frac{\dot{\varepsilon}_p}{\dot{\varepsilon}_p^r} \right) \right] \left[1 - \Theta^m \right] \tag{9}$$

Where

$$\Theta = \begin{cases} 0 & for \quad T < T_r \\ \dfrac{T - T_r}{T_m - T_r} & for \quad T_r < T < T_m \\ 1 & for \quad T > T_m \end{cases} \tag{10}$$

The parameters are summarized in Table 3.

Table 3 JC parameters for cold rolled 1020 steel in dynamic shear at ~10^3–10^4 1/s

A [MPa]	B [MPa]	n	C	m	Tr [C°]	Tm [C°]	$\dot{\varepsilon}_p^r$	ε_p^f ductility
500	227	0.41	0.04	1.0	25	1456	1	0.8

References

1. Gray GT, Vecchio KS, Livescu V (2016) Compact forced simple-shear sample for studying shear localization in materials. Acta Mater, 103, 12–22.

2. Rogers HC (1979) Adiabatic plastic deformation. Annu Rev Mater Sci 9(1):283–311
3. Vural M, Ravichandran G, Rittel D (2003) Large strain mechanical behavior of 1018 cold-rolled steel over a wide range of strain rates. Metall Mater Trans A 34(12):2873–2885
4. Clausen A, Børvik T, Hopperstad OS, & Benallal A (2004) Flow and fracture characteristics of aluminium alloy AA5083–H116 as function of strain rate, temperature and triaxiality. Mat Sci Eng: A 364(1):260–272.
5. Børvik T, Hopperstad OS, Berstad T (2003) On the influence of stress triaxiality and strain rate on the behaviour of a structural steel. Part II numerical study. Eur J Mech – A. Solids 22(1):15–32
6. Johnson GR, & Cook WH (1985) Fracture characteristics of three metals subjected to various strains, strain rates, temperatures and pressures. Eng Fract Mech 21(1):31–48
7. Wierzbicki T, Bao Y, Lee Y.-W., Bai Y (2005) Calibration and evaluation of seven fracture models. Int J Mech Sci, vol. 47, no. 4–5, pp. 719–743
8. Hopperstad OS, Børvik T, Langseth M, Labibes K, Albertini C (2003) On the influence of stress triaxiality and strain rate on the behaviour of a structural steel. Part I experiments. Eur J Mech – A Solids 22(1):1–13
9. Markiewicz É, Langrand B, Notta-Cuvier D (2017) A review of characterisation and parameters identification of materials constitutive and damage models: from normalised direct approach to most advanced inverse problem resolution. Int J Impact Eng. in press. https://doi.org/10.1016/j.ijimpeng.2017.01.028
10. Mohr D, Oswald M (2008) A new experimental technique for the multi-axial testing of advanced high strength steel sheets. Exp Mech 48(1):65–77
11. Klepaczko JR (1996) Plastic shearing at very high strain rates, a review. In Constitutive relation in high/very high strain rates. Tokyo: Springer Japan, pp. 59–68
12. Dodd B, Bai Y (Eds.) (2012) Adiabatic shear localization : frontiers and advances. Elsevier
13. Gilat A, Wu X (1997) Plastic deformation of 1020 steel over a wide range of strain rates and temperatures. Int J Plast 13(6–7):611–632
14. Couque H (2003, September) A hydrodynamic hat specimen to investigate pressure and strain and strain rate dependence on adiabatic shear band formation. J Phys IV (Proc) (Vol. 110, pp. 423–428). EDP sciences
15. Peirs J, Verleysen P, Degrieck J. The use of hat - shaped specimens for dynamic shear testing. Found Civil Environ Eng (11):97–111
16. Peirs J, Verleysen P, Degrieck J, Coghe F (2010) The use of hat-shaped specimens to study the high strain rate shear behaviour of Ti–6Al–4V. Int J Impact Eng 37(6):703–714
17. Pepelnjak T, Magoč V, Barišić B (2012) Analysis of shear hat test in digital environment. Metalur-Zagreb 51(2):153
18. Dorogoy A, Karp B, Rittel D (2011) A shear compression disk specimen with controlled stress triaxiality under quasi-static loading. Exp Mech 51(9):1545–1557
19. Karp B, Dorogoy A, Rittel D (2013) A shear compression disk specimen with controlled stress triaxiality under dynamic loading. Exp Mech 53(2):243–253
20. Dunand M, Mohr D (2011) Optimized butterfly specimen for the fracture testing of sheet materials under combined normal and shear loading. Eng Fract Mech 78(17):2919–2934
21. Peirs J, Verleysen P, Degrieck J (2012) Novel technique for static and dynamic shear testing of Ti6Al4V sheet. Exp Mech 52(7):729–741
22. Nicholas T (1981) Tensile testing of materials at high rates of strain. Exp Mech 21(5):177–185
23. Rittel D, Lee S, Ravichandran G (2002) A shear-compression specimen for large strain testing. Exp Mech 42(1):58–64
24. Dorogoy A, Rittel D, Godinger A (2015) Modification of the shear-compression specimen for large strain testing. Exp Mech 55(9): 1627–1639
25. Dorogoy A, Rittel D, Godinger A (2016) A shear-tension specimen for large strain testing. Exp Mech 56(3):437–449
26. Simulia (2014) Abaqus/CAE version 6.14–2 (2014). Dassault Systèmes Simulia Corp., Providence, RI, USA
27. Simulia (2014) Abaqus/Explicit Version 6.14–2, Abaqus documentation. Dassault systemes, 2014
28. Barsoum I, Faleskog J (2007) Rupture mechanisms in combined tension and shear—experiments. Int J Solids Struct 44(6):1768–1786
29. Bai Y, Wierzbicki T (2008) A new model of metal plasticity and fracture with pressure and lode dependence. Int J Plast 24(6):1071–1096
30. Johnson GR, & Cook WH (11983, April) A constitutive model and data for metals subjected to large strains, high strain rates and high temperatures. Proc 7th Int. Symp Ballistics (Vol. 21, No.1, pp. 541–547)
31. Gautam SS, & Saxena RK (2012) A numerical study on effect of strain rate and temperature in the Taylor rod impact problem. J Struct Chang Solids 4:1–11